MNRAS **000**, 1–8 (2019) Preprint 19 June 2020 Compiled using MNRAS LATEX style file v3.0

Eclipse-time analysis in AA Dor observed with *TESS* satellite

A.S. Baran,[1,2]★ R.H. Østensen,[1,2,3]
[1]*ARDASTELLA Research Group, Institute of Physics, Pedagogical University of Krakow, ul. Podchorążych 2, 30-084 Kraków, Poland*
[2]*Department of Physics, Astronomy, and Materials Science, Missouri State University, Springfield, MO 65897, USA*
[3]*Recogito AS, Storgaten 72, N-8200 Fauske, Norway*

Accepted XXX. Received YYY; in original form ZZZ

ABSTRACT
We present our analysis of *TESS* photometry of AA Dor. This star has been monitored for almost one year and such long time-series data were subject to stellar pulsations search and eclipse timing analysis. The pulsations were not detected down to 0.07 ppt. The mid-times of eclipses allowed us to confirm a very stable orbital period, with an upper limit of orbital period change to be $5.75{\cdot}10^{-13}$ s/s. Neither tertiary companion nor mass exchange is expected in this system. The offset of the secondary eclipse is caused purely by the Rømer delay and confirms that the mass of the primary is consistent with a canonical mass of EHB stars, while the secondary mass to be at the limit of hydrogen burning.

Key words: binaries: general subdwarfs, stars: oscillations (including pulsations), stars: eclipsing binaries, stars: individual (AA Dor)

1 INTRODUCTION

Subdwarf B (sdB) stars are identified as compact stars located on the blue extension of the horizontal branch (EHB). The progenitors of sdB stars are Sun-like stars but must have lost significant mass during or immediately after their ascent of the red-giant branch, leaving them with only a tiny remnant of their hydrogen envelopes. The mass loss must happen before helium ignition, otherwise they would become normal horizontal branch stars (Heber 2016). Binary population synthesis modelling have been performed exploring various different mass-loss scenarios, as detailed by Han et al. (2002). Several channels exist, depending on the initial configuration of the system, and depending on the mass ratio, the binary system ends up either in a wide orbit (via stable Roche lobe overflow, when the companion is sufficiently massive) or a close orbit (after common-envelope ejection, when the companion is of lower mass than the stripped EHB star). Since EHB stars must have a mass close to the core-helium flash mass of 0.5 $M_\odot$ masses, the close-orbit systems can only consist of an sdB with either an M dwarf (dM), brown dwarf, or white dwarf companion.

HW Vir is the class prototype for the sdB+dM systems (Menzies & Marang 1986). Wolz et al. (2018) provided a list of all HW Vir systems studied prior to 2018. It contains 20 systems including those with brown dwarfs as secondaries. A large number of faint HW Vir candidates from ground-based photometric surveys was recently published by Schaffenroth et al. (2019). A typical light curve of HW Vir systems shows two distinct eclipses and an out-of-eclipse variation, explained by an irradiation effect. The eclipses indicate a nearly edge-on orbital orientation (inclination close to 90°). Eclipse mid-times can be used to study the stability of the orbital period, sometimes leading to the discovery of periodic modulations in the eclipse timings, which is indicative of additional companions (e.g. Baran et al. 2015).

HW Vir systems are important objects for testing the proposed evolutionary channels of sdB stars by Han et al. (2002). Deriving the masses of both components is therefore crucial, but difficult. HW Vir systems are usually single-line spectroscopic binaries, since the secondary companions are not easily detectable in the presence of more luminous hot stars. The luminosity ratio is of the order of 10^6. Masses of sdB stars are frequently assumed to be close to 0.47 $M_\odot$ (Fontaine et al. 2012), which is often referred to as the canonical mass. In fact, a narrow range of helium core masses is typical for a wide mass range of progenitors (0.7–1.9 $M_\odot$) that undergo a helium flash. This means the canonical mass of about 0.47 $M_\odot$ likely a valid assumption. However, there is also the chance that an sdB's mass could be down to 0.31 $M_\odot$, produced by a narrow range of progenitor masses close to 1.9–2.2 $M_\odot$, and for a wider range (2.2–3.7 $M_\odot$) of progenitors that ignite helium under non-degenerate conditions. Those values are given for a specific set of parameters (mainly metallicity) and more details on this calculation will be provided in another paper. The dependence on metallicity and other parameters leads us to conclude that assuming a canonical mass for an sdB star is not necessarily correct, and may lead to an incorrect mass estimation of the secondary component in HW Vir systems. Stellar oscillations predicted and discovered in sdB stars by Charpinet et al. (1997) and Kilkenny et al. (1997), respectively, are potentially useful toward sdB mass estimations. Asteroseismology uses pulsation properties to describe stellar interiors. An recent example of a mass estimation is Charpinet et al. (2019). Surprisingly, the estimated mass is 0.39 $M_\odot$, so not a canonical mass. Other

★ E-mail: andrzej.baran@up.krakow.pl

derived masses have been closer to the canonical one, (see for example Charpinet et al. 2011; Baran et al. 2019). Models which predict unstable pulsation modes in sdBs were first published by Charpinet et al. (1997). To date, the sample of pulsating sdB stars is approaching a hundred, with half of the sample discovered during the space photometry missions *Kepler*, *K2* and *TESS*.

Binary systems provide an independent tool to estimate masses. In the case of HW Vir systems, the masses are not easily derived, since a significant temperature difference between components makes it difficult to see the secondary/fainter companion and then the mass estimation for the secondary is based on an assumption of the primary having the canonical mass, which may not always be correct. Kaplan (2010) reported of a new tool to estimate masses in binary systems. He showed that, even in the case of a circular orbit, a secondary eclipse is not centered at 0.5 orbital phase, a.k.a. the Rømer delay. The predicted delay may be of just a few seconds, and therefore very precise data, which allow for precise eclipse mid-times derivation, are required. Barlow et al. (2012) measured that shift in 2M 1938+4603, one of the systems observed by the *Kepler* spacecraft. They measured the delay to be below 2 s and consequently the mass of the primary to be 0.37 $M_\odot$. Next, Baran et al. (2015) used a longer time span and arrived at a slightly smaller shift. These authors reported the mass of the secondary to be smaller than 0.3 $M_\odot$, which is contrary to the canonical mass. However, both Barlow et al. (2012) and Baran et al. (2015) noted that the eccentricity of the orbit may also contribute to the offset of the secondary eclipse and the overall shift may not be pure Rømer delay. In that case, the mass estimation may not be correct. Baran et al. (2018) reported an attempt of an application of the Rømer delay to the HW Vir system. The mass the authors derived was similar to that of 2M 1938+4603. They also arrived at the same conclusion about eccentricity. These three cases showed that the idea of Kaplan (2010) is very tough to be employed conclusively since the unconstrained eccentricity does not allow for reasonably precise mass derivations.

A primary mass around 0.3 $M_\odot$ raises a question on the nature of this component. Such a low mass cannot be obtained for a He-core burning HB star (J.Ostrowski - private communication). Instead, if the mass of 0.3 $M_\odot$ is correct, those objects will be non-core-helium burning post RGB stars, which have lost too much mass before the helium flash and will head directly toward the low mass white dwarf cooling track. Baran et al. (2018) presented a discussion toward this interpretation of the primary in HW Vir system.

2M 1938+4603 and HW Vir were observed during the *Kepler* mission, which provided continuous time-series data of unprecedented quality, which was good enough to estimate the shift of the secondary eclipse. Another HW Vir-like system observed during a space mission is AA Dor. It was observed during 13 months by the *TESS* satellite. A flux variation of AA Dor was first reported by Kilkenny & Hill (1975) and this system has subsequently been frequently studied. The light curve of AA Dor resembles that of HW Vir though because the estimated mass of the fainter component falls below the hydrogen core burning stellar configuration, the secondary was considered to be a brown dwarf. Since the effective temperature and surface gravity placed the AA Dor primary inside the EHB region, the primary mass was assumed to be 0.5 $M_\odot$. To determine the masses reliably one needs to detect spectral lines of both components. A spectroscopic effort to determine the nature of the secondary component was undertaken *e.g.* by Hilditch et al. (1996) and Rauch & Werner (2003). No definite conclusion has been achieved, since the mass of the primary had to be assumed upfront. Vučković et al. (2008) re-analyzed the spectroscopic data of Rauch & Werner (2003) discovering emission lines originating from the heated side of the secondary. The authors made the first estimate of the masses of both AA Dor components, which were consistent with a regular EHB primary and a low-mass M dwarf secondary. A subsequent effort by Klepp & Rauch (2011) ruled out the post-RGB channel. Most recent work by Hoyer et al. (2015) and Vučković et al. (2016) brought, to date, the best estimations of radial velocity amplitudes of both components, allowing for precise mass determinations of both components. Both authors cited radial velocity amplitudes and corresponding masses that agree, within the errors, though the uncertainty of the radial velocity amplitude of the secondary component reported by Vučković et al. (2016) is an order of magnitude smaller. The masses indicate that the primary star is close to canonical, and the secondary is on the limit of hydrogen burning for a main sequence star.

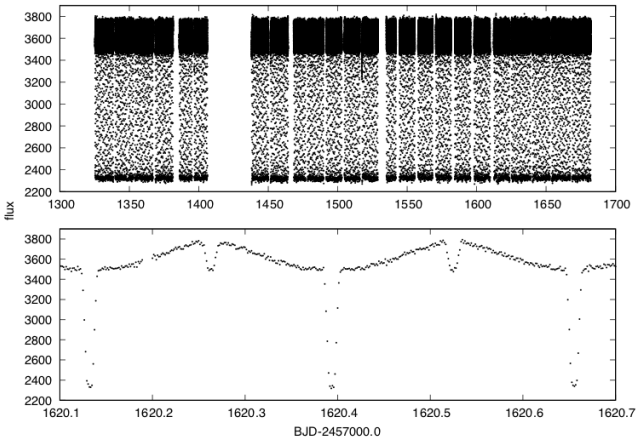

Figure 1. Light curve of AA Dor obtained by *TESS* during Year 1 of the mission. The top panel shows the entire processed data set, while the bottom panel shows the flux variations during a couple of orbital periods.

We report results of our work on *TESS* photometric data of AA Dor. We searched for stellar pulsations in the AA Dor primary, did an analysis of orbital period stability, and measured the shift of the secondary eclipse, which we applied to estimate masses of both components.

2 TESS PHOTOMETRIC DATA

AA Dor (α_{2000} = 05^{h}31^{m}40.36^s, δ_{2000} = −69°53′02.2″) was observed during the first cycle of the near all-sky survey undertaken with the Transiting Exoplanet Survey Satellite (*TESS*). *TESS* is deployed in an elliptical, 2:1 lunar synchronous orbit with a period of 13.7 d. Each annual cycle of *TESS* observations are split up into sectors lasting two orbits, or about 27 d. The detector consists of four contiguous CCD cameras, each covering a 24° x 24° field of view (FoV), making up a 24° x 96° strip aligned along ecliptic latitude lines. The data are stored with the short cadence (SC), lasting 120 s and the long cadence (LC), lasting 1800 s. When one sector's observations have been completed, the instrument FoV is shifted eastward by 27°, naturally pivoting around the ecliptic pole. It takes 13 sectors to pivot around one pole, then the FoV is shifted to the other hemisphere for the next cycle. As a result, the regions near the ecliptic poles are observed during every sector and are known as the continuous viewing zones of *TESS*. Luckily, AA Dor is located in this zone around the southern ecliptic pole. We downloaded all available data from the "Barbara A. Mikulski Archive for Space

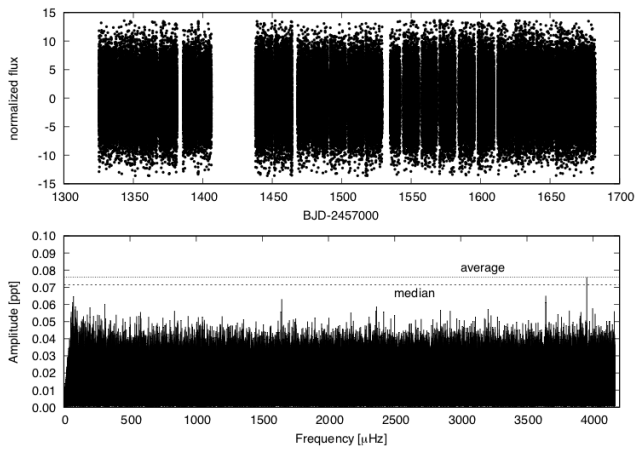

Figure 2. Top panel: residuals of prewhitening and clipping. Bottom panel: amplitude spectrum up to the Nyquist frequency (4166 μHz). The dashed and dotted lines in the bottom panel represent the 5σ detection threshold calculated using median (0.715 ppt) and average (0.760 ppt), respectively.

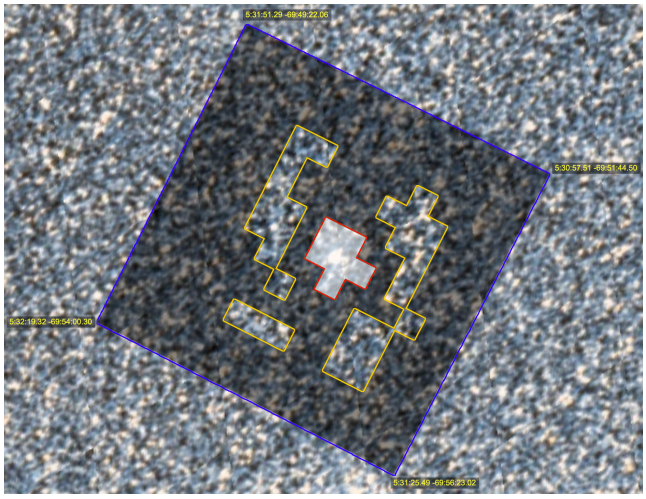

Figure 3. Image showing the a part of the sky around AA Dor. The red aperture is used for the target flux, while the yellow one is used for the sky background estimation.

Telescopes" (MAST)[1]. The data span all 13 sectors with the exception of Sector 4, during which AA Dor was not included in the target list. We used the SC data which has a time resolution high enough to allow us to sample the eclipses and to search for stellar pulsations up to 4166 μHz, covering both the g-mode and partially the p-mode regions in an amplitude spectrum. We extracted PDCSAP_FLUX, which is corrected for on-board systematics and neighbors' contribution to the overall flux. We clipped fluxes at 5σ to remove outliers, de-trended long term (of the order of days) variation with polynomials. We show the resultant light curve in Figure 1.

3 STELLAR PULSATIONS

A few of the sdB primaries in HW Vir systems show stellar pulsations. The examples are NY Vir, 2M 1938+4603 and HW Vir. Therefore, we made an attempt to detect stellar pulsations in AA Dor. The light curve of AA Dor is dominated by eclipses and an irradiation effect. In order to detect any pulsations, which would typically have amplitudes close to the 10 ppt level, we had to remove the binary orbit signature from the data. First, we used a Fourier domain to calculate the binary frequency and a sequence of harmonics, which show up as a consequence of a non-sinusoidal shape of the flux variation. Then, we prewhitened the binary frequency along with 93 harmonics, and finally clipped the residuals to remove data points that became outliers after prewhitening. We present the result of this data processing in Figure 2. The light curve no longer shows any binary trend. The amplitude spectrum is fairly smooth with just a few low amplitude frequencies. The highest amplitude one is detected at 3952.19 μHz. It meets the 5σ criterion if we use averaging to calculate the mean noise level. However, if the median is used, that frequency is not significant. Regardless of the method, we accept that one frequency is not sufficiently convincing and therefore we make no claim for or against the AA Dor primary to be a pulsator. Higher precision data are required to make a convincing conclusion.

The AA Dor primary, with an effective temperature of 42 000 K (Rauch 2000), is on the hot end of known sdB pulsators, where few have been located. Exceptions have been the sdO (Woudt et al. 2006) and ω Cen pulsators (Brown et al. 2013). Temperatures between 40,000 and 50 000 K may not allow for observable pulsation amplitudes with currently available time-series data sets. Another reason may be that the amplitudes are diluted by an overestimated flux level. The pulsation amplitudes in other HW Vir system primaries, are around 0.1 ppt. If the AA Dor primary has amplitudes below 0.1 ppt, they will be diluted to lower levels since AA Dor is located in front of a dense stellar environment, namely the Large Magellanic Cloud. In Figure 3 we show a part of the sky around AA Dor with the target mask and the optimal aperture overplotted. This figure clearly shows that the CCD pixels used in the optimal aperture for the target overestimate AA Dor 's flux while those used for sky background overestimate the true sky flux. This leads to a dilution in amplitude of any flux variations in AA Dor.

AA Dor has also been observed with the *Gaia* satellite. The parallax was measured as 2.72 (6) mas, which translates to a distance of 368 (8) parsecs. The *Gaia* G-band magnitude was estimated to be 11.16 (Gaia Collaboration 2018).

4 THE MID-TIMES OF ECLIPSES

Flux variations caused by orbital motion include two eclipses and an irradiation effect. The eclipses are used to study the stability of the orbital period. The mid-times of eclipses are plotted in the so-called *Observed minus Calculated* (O–C) diagram, which can be used to measure an orbital period variation (Sterken 2005). Its variability provides clues on *e.g.* possible mass exchange, a tertiary body, or gravitational wave radiation. To calculate mid-times we used the method described in Kwee & van Woerden (1956). Since we detected no significant pulsations, eclipse shapes are not distorted by other variability and strictly defined by the geometry of the system. However, to increase the sampling during eclipses and to lower uncertainties of the mid-times, we decided to fold a part of the light curve obtained during a single *TESS* orbit over the binary period calculated from individual eclipses. This folding increases precision of data in an O–C diagram, paying the price of decreased time resolution, since the total number of eclipses is decreased to

[1] archive.stsci.edu

Table 1. The orbital period of AA Dor derived since its discovery.

Period [days]	Uncertainty	Reference
0.261539	0.17 sec	Kilkenny et al. (1978)
0.2615398	17 msec	Kilkenny et al. (1979)
0.261539724	0.35 msec	Kilkenny (1983)
0.261539726	0.26 msec	Kilkenny (1986)
0.2615397198	0.15 msec	Kilkenny et al. (1991)
0.261539731	0.17 msec	Kilkenny et al. (2000)
0.2615397363	35 µsec	Kilkenny (2011)
0.2615397323	0.35 msec	this work

24. However, we do not expect any orbital period variation on a time scale of days or less. In addition, we binned data in each eclipse to end up with 30 points per eclipse. We show the result of our light curve folding in Figure 4.

Having folded the light curve, we recalculated the ephemeris from primary eclipses and obtained

$$T_{pri} = 2455681.9153693\,(32)\,\mathrm{BJD} + 0.2615397323\,(40)\,\mathrm{E}$$

Likewise, we re-calculated the ephemeris from secondary eclipses and obtained

$$T_{sec} = 2455682.046202\,(9)\,\mathrm{BJD} + 0.261539724\,(11)\,\mathrm{E}$$

The orbital periods derived from both types of eclipses agree very well to within the errors. We plot the O-C diagrams for primary and secondary eclipses in Figure 5.

The orbital period has been monitored for tens of years. In Table 1 we list values of the orbital period derived over time along with its uncertainty. Dave Kilkenny of South African Astronomical Observatory and his collaborators have been very active in this field. The consecutive values of the orbital period are derived from all mid-times available to the authors. We can see how a longer time baseline helps increase the precision of the orbital period. Kilkenny (2011) presented the most precise orbital period and the O–C analysis, which shows that the orbital period remains very stable over 30 years of monitoring (their Figures 1 and 2). Our work confirms that the orbital period remains stable. The period difference between 1981 and 2019 is 0.69 msec, which gives an upper limit for period change to be $5.75{\cdot}10^{-13}$ s/s. The O–C diagram does not indicate any tertiary body in the system, while other effects, which could cause period change, are negligible.

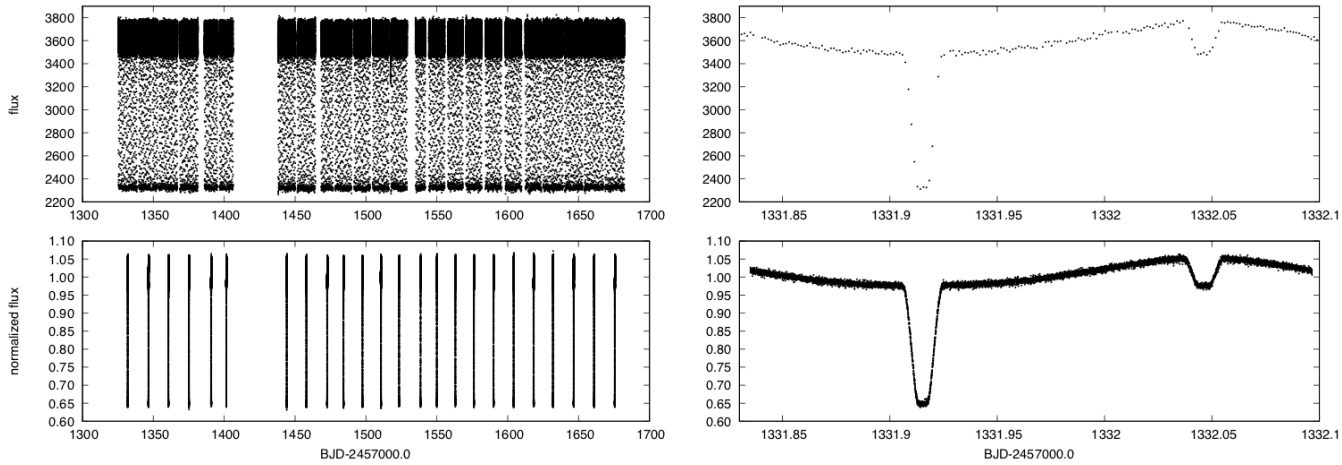

Figure 4. Left upper panel shows the original light curve, while left bottom one shows the light curve folded over each *TESS* orbit. Upper right panel shows a close-up of an unfolded eclipse, while right bottom one shows a folded one.

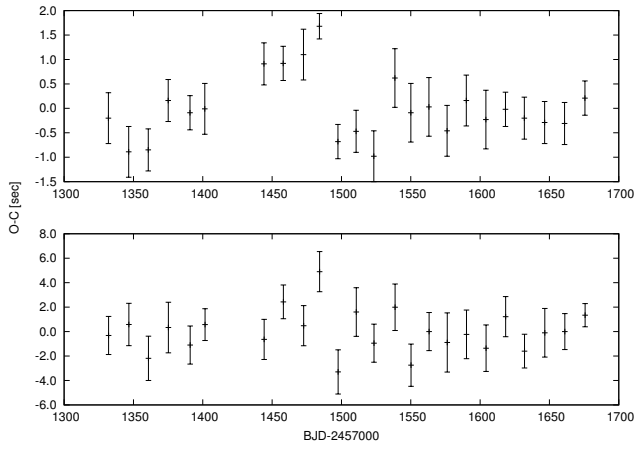

Figure 5. The O-C diagrams for primary (upper panel) and secondary (bottom panel) eclipses.

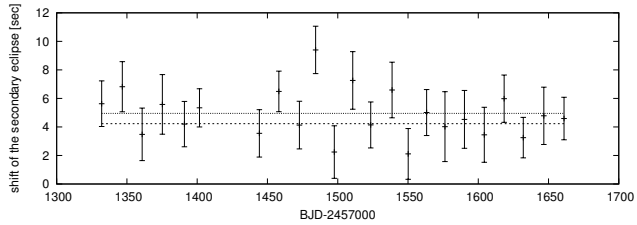

Figure 6. The shift of the secondary eclipse measured in folded and binned eclipses. Two horizontal lines show the range of the mean value of the shift.

5 SHIFT OF THE SECONDARY ECLIPSE

Binary systems with components of unequal masses must show the mid-times of secondary eclipses to happen slightly later than half an orbital phase after the primary eclipses. The effect is caused by the finite speed of light and is often called the Rømer delay. This shift must be present unless the masses of both components are equal or the orbit has a specifically-tuned eccentricity which cancels out the shift. In the case of circular orbits, the offset of the secondary eclipse is purely due to the Rømer delay, thus it provides a direct measure of the mass ratio, when the orbital velocity of either component and the orbital period, P, are known. All these quantities can be measured, so the mass estimates are purely observational and do not require any modeling or calibrations. All necessary formulae can be found, *e.g.* in Baran et al. (2018).

We calculated the shifts from 24 folded and binned primary and secondary eclipses. Then we took a mean value, which we found to be 4.59 (36) s. The uncertainty is defined as a standard deviation of the mean value. We plotted our calculated shifts, along with the range of the mean value in Figure 6. Since Hoyer et al. (2015) and Vučković et al. (2016) reported the values of the radial velocity amplitudes of both components, we can calculate the expected shift of the secondary eclipses, assuming the orbit remains circular. Hoyer et al. (2015) cited a value of K_2 to be $232.9^{16.6}_{-6.5}$ km/s and K_1 to be 40.15 (11) km/s. Vučković et al. (2016) cited K_2 to be 231.3 (7) km/s and K_1 to be 39.63 (21) km/s, both derived from their analysis. The uncertainty of K_2 cited by Vučković et al. (2016) is smaller and therefore we used it in our analysis. The uncertainty of K_1 is smaller, however, it was derived with the assumption of an eccentric orbit. Three additional free parameters make the fit better, and reduce the errors of the fitted parameters. However, both cited values are almost identical and make no difference in our results. Therefore, for consistency, we adopted values of K_1 and K_2 values and consequently, the mass ratio, from Vučković et al. (2016). We adopted the orbital period from our ephemeris, calculated from folded primary eclipses. The expected shift of the secondary eclipses equals 4.599 (28) s. This value agrees perfectly with the one we derived from our observations, measuring the shift directly from the secondary eclipses.

Table 2. Known HW Vir systems and new candidates observed with *TESS*. Only systems observed with either *TESS* or *K2* in SC mode have been included.

Name	V* name	TIC	P d	K_1 km/s	G mag	Plx mas	Reference
J19447+5449		467187065	0.0642	-	15.78	0.59	New
KPD 2045+5136		365213081	0.0896	-	15.23	0.95	New
HE 0516-2311		408187719	0.0912	-	15.93	0.50	New
PTF1 J011339...		611402948	0.0934	74.2	16.65	0.70	Wolz et al. (2018)
HS 0705+6700	V470 Cam	99641129	0.0956	85.8	14.62	0.81	Drechsel et al. (2001)
SDSS J0820+0008		455206965	0.0962	47.4	15.18	0.66	Geier et al. (2011)
PG 1336–018	NY Vir	175402069	0.1010	78.6	13.39	1.81	Vučković et al. (2007)
J19065+2807		281948821	0.1121	-	15.65	0.54	New
BD–07°3477	HW Vir	156618553	0.1168	82.3	10.61	5.80	Baran et al. (2018)
EC 10246–2707		193092806	0.1185	71.6	14.44	0.90	Barlow et al. (2013)
2M1938+4603		271164763	0.1258	65.7	12.14	2.50	Østensen et al. (2010)
J14019–7513		396004353	0.1315	-	13.53	1.78	New
ASAS 10232–3737		73764693	0.1393	81.0	11.71	3.74	Schaffenroth et al. (2013)
2M 1533+3759		148785530	0.1618	71.1	12.98	1.90	For et al. (2010)
J21469+6616		322390461	0.1935	-	16.22	0.72	New
FBS 0747+725		441613385	0.2083	-	16.52	0.49	Pribulla et al. (2013)
LB 3459	AA Dor	425064757	0.2615	39.2	11.16	2.72	Vučković et al. (2016)
EC 23068–4801		139266474	0.2641	-	15.39	0.65	New
Ton 301		165797593	0.3697	-	13.80	1.19	New
EC 02406–6908		259864042	0.4607	-	14.67	0.86	New

6 DISCUSSION

We derive values for the masses of 0.46 (5) $M_\odot$ and 0.079 (9) $M_\odot$ for the primary and the secondary components, respectively. The masses are in agreement with those derived by both Hoyer et al. (2015) and Vučković et al. (2016) and confirms that the primary has the same mass as normal EHB stars. The orbit of AA Dor is likely circular. If the orbit were eccentric, it would contribute to the shift of secondary eclipses according to Equation 8 in Baran et al. (2018). There are two parameters that are essential, eccentricity e and the argument of pericentre, ω. If the value of e is non-zero and ω is different from $\pi/2$ or $3\pi/2$, the shift we derived from eclipses would be bigger or smaller depending on the sign of $\cos\omega$. While we cannot completely rule out a non-zero eccentricity, if the orbit were eccentric, while $\cos\omega$ is close to zero, the contribution to the shift of the secondary eclipse would remain negligible, so the shift of the secondary agrees well with the Rømer delay. Unfortunately, a small eccentricity is not detectable in current observations so a definite conclusion cannot be made. Perhaps, an apsidal motion caused by a precession of an eccentric orbit would help to set the limit on eccentricity, however thus far observations do not indicate that this could be the case. Convincing observations are yet to be collected.

We have also searched for new HW Vir systems in *TESS* SC data, and nine excellent candidates have been found (Table 2). All these systems were targeted in SC mode due to either being known sdB stars, or candidates from the Geier et al. (2017) Gaia-selected subdwarf sample. Although these stars are certainly worth closer follow-up spectroscopy, none of them are in the continuous viewing zone, and therefore the length of the *TESS* observations are limited to one or two months. Note that the two new systems with periods longer than that of AA Dor would be particularly welcome targets for Rømer delay measurements, since the delays would be more significant in the wider orbits. TON 301 is an excellent new target for monitoring by the Northern observatories. On the other hand, EC 02406–6908 has a very shallow grazing secondary eclipse, making observations challenging. The folded light curves of nine new HW Vir systems calculated from photometry taken with *TESS* are plotted in Figure 7.

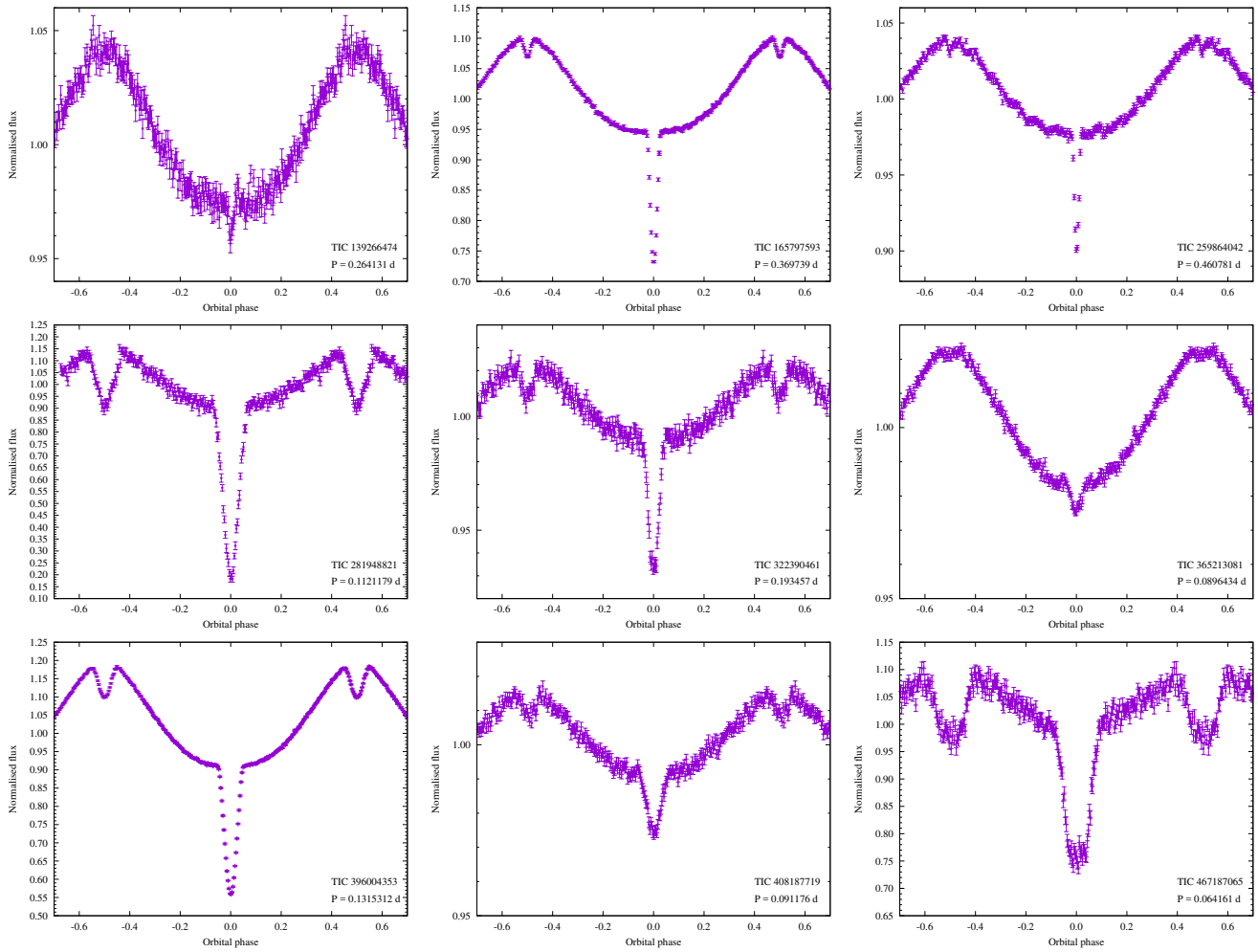

Figure 7. The folded light curves of nine new HW Vir candidate systems we found in *TESS* photometry.

7 SUMMARY

We have presented new photometric observations of AA Dor collected with the *TESS* satellite. Since AA Dor is located in TESS's southern continuous viewing zone, we obtained a total of 12 sectors of data spanning just over one year. AA Dor is a close binary system consisting of a hot primary and a cool companion. The light curve shows variations caused by mutual eclipsing and an irradiation effect. As in other HW Vir systems, we searched for stellar pulsations in the hot primary, though with a null result. The reason may be twofold. The primary is hotter than those in other systems, which does not favor the driving mechanism, and the *TESS* data precision is lower than *Kepler* data, making a higher positive detection limit.

We have analysed eclipses by deriving their mid-times and calculating an O–C diagram. This analysis confirmed a very stable orbital period with a limit on the period change to be not faster than $5.75{\cdot}10^{-13}$ s/s. Such a value excludes a tertiary body in the system, as well as any significant mass exchange. We have also measured a shift of the secondary eclipse. There are only a few other sdB stars for which the shift of the secondary eclipse has been derived. Baran et al. (2015) reported a shift of 1.76 s for 2M 1938+4603 after it had been observed for three years with the *Kepler* spacecraft, Baran et al. (2018) reported a shoft of 1.509 sec for HW Vir based on *K2* data, and another two stars were reported by Schaffenroth et al. (2015) and Lee et al. (2017) using ground-based data, yet neither had sufficient precision to derive a precise shift. The shifts in 2M 1938+4603 and HW Vir are too small to reproduce canonical masses for the primaries. It was suggested that either the mass is truly low and the primaries are low-mass post RGB stars which have not gone through a helium flash, or the shifts are affected by non-zero eccentricity that is too small to be confirmed by current observations. AA Dor is the first case when the shift agrees with the prediction based on a radial velocity amplitude of the cool companion. This amplitude was derived neither for 2M 1938+4603 nor HW Vir. The shift in AA Dor confirms the nature of the primary companion to be an EHB object with a canonical mass of 0.46 $M_{\odot}$, and the secondary companion to be at the limit of nuclear burning. In fact, the mass of the secondary is just below the limit, though the uncertainties do not allow for a definite conclusion.

ACKNOWLEDGEMENTS

Financial support from the Polish National Science Centre under projects No. UMO-2017/26/E/ST9/00703 and UMO-2017/25/B/ST9/02218 is appreciated. This work presents results

from the European Space Agency (ESA) space mission *Gaia*. *Gaia* data are being processed by the *Gaia* Data Processing and Analysis Consortium (DPAC). Funding for the DPAC is provided by national institutions, in particular the institutions participating in the *Gaia* MultiLateral Agreement (MLA). The *Gaia* mission website is https://www.cosmos.esa.int/gaia. The *Gaia* archive website is https://archives.esac.esa.int/gaia. This research was made possible through the use of the AAVSO Photometric All-Sky Survey (APASS), funded by the Robert Martin Ayers Sciences Fund. This paper includes data collected by the *TESS* mission. Funding for the *TESS* mission is provided by the NASA Explorer Program.

REFERENCES

Baran A., Zola S., Blokesz A., Østensen R., Silvotti R., 2015, A&A, 577, 146
Baran A., et al., 2018, MNRAS, 481, 2721
Baran A., Telting J., Jeffery C., Østensen R., Vos J., Reed M., Vučković M., 2019, MNRAS, 489, 1556
Barlow B., Wade R., Liss S., 2012, ApJ, 753, 101
Barlow B. N., et al., 2013, MNRAS, 430, 22
Brown T., Landsman W., Randall S., Sweigart A., T. L., 2013, ApJ, 777, 22
Charpinet S., Fontaine G., Brassard P., Chayer P., Rogers F. J., Iglesias C. A., Dorman B., 1997, ApJ, 483, 123
Charpinet S., et al., 2011, A&A, 530, 3
Charpinet S., et al., 2019, A&A, 632, 90
Drechsel H., et al., 2001, A&A, 379, 893
Fontaine G., Brassard P., Charpinet S., Green E. M., Randall S. K., Van Grootel V., 2012, A&A, 539, 12
For B.-Q., et al., 2010, ApJ, 708, 253
Gaia Collaboration 2018, A&A, 616, A10
Geier S., et al., 2011, ApJ, 731, L22
Geier S., Østensen R. H., Nemeth P., Gentile Fusillo N. P., Gänsicke B. T., Telting J. H., Green E. M., Schaffenroth J., 2017, A&A, 600, A50
Han Z., Podsiadlowski P., Maxted P. F. L., Marsh T. R., Ivanova N., 2002, MNRAS, 336, 449
Heber U., 2016, PASP, 128, 2001
Hilditch R. W., Harries T. J., Hill G., 1996, MNRAS, 279, 1380
Hoyer D., Rauch T., Werner K., Hauschildt P., Kruk J., 2015, A&A, 578, 125
Kaplan D., 2010, ApJ, 717, 108
Kilkenny D., 1983, SAAOC, 7, 55
Kilkenny D., 1986, The Observatory, 106, 160
Kilkenny D., 2011, MNRAS, 412, 487
Kilkenny D., Hill P. W., 1975, MNRAS, 173, 625
Kilkenny D., Hilditch R., Penfold J., 1978, MNRAS, 183, 523
Kilkenny D., Lynas-Gray A., Hilditch R., 1979, in van Horn H., Weidemann V., eds, White Dwarfs and Variable Degenerate Stars. Proceedings of IAU Colloq. 53. p. 255
Kilkenny D., Harrop-Allin M., Marang F., 1991, IBVS, 3569, 1
Kilkenny D., Koen C., O'Donoghue D., Stobie R. S., 1997, MNRAS, 285, 640
Kilkenny D., Keuris S., Marang F., Roberts G., van Wyk F., Ogloza W., 2000, The Observatory, 120, 48
Klepp S., Rauch T., 2011, A&A, 531, 7
Kwee K., van Woerden H., 1956, Bulletin of the Astronomical Institutes of the Netherlands, 12, 327
Lee J., Youn J.-H., Hong K., Han W., 2017, ApJ, 839, 39
Menzies J., Marang F., 1986, in Hearnshaw J., Cottrell P., Reidel Dordrecht eds, Instrumentation and Research Programmes for Small Telescopes. Proceedings of the International Astronomical Union Symposium No. 118. p. 305
Østensen R., et al., 2010, MNRAS, 408, 51
Pribulla T., et al., 2013, Information Bulletin on Variable Stars, 6067, 1
Rauch T., 2000, A&A, 356, 665
Rauch T., Werner K., 2003, A&A, 400, 271
Schaffenroth V., Geier S., Drechsel H., Heber U., Wils P., Østensen R. H., Maxted P. F. L., di Scala G., 2013, A&A, 553, A18
Schaffenroth V., Barlow B., Drechsel H., Dunlap B., 2015, A&A, 576, 123
Schaffenroth V., et al., 2019, MNRAS, 630, 80
Sterken C., 2005, in Sterken C., ed., Astronomical Society of the Pacific Conference Series Vol. 335, The Light-Time Effect in Astrophysics. p. 3
Vučković M., Østensen R., Bloemen S., Decoster I., Aerts C., 2008, in Heber U., Jeffery C. S., Napiwotzki R., eds, Astronomical Society of the Pacific Conference Series Vol. 392, Hot Subdwarf Stars and Related Objects. p. 199
Vučković M., Østensen R., Németh P., Bloemen S., Pápics P., 2016, A&A, 586, 146
Vučković M., Aerts C., Østensen R., Nelemans G., Hu H., Jeffery C. S., Dhillon V. S., Marsh T. R., 2007, A&A, 471, 605
Wolz M., et al., 2018, Open Astronomy, 27, 80
Woudt P., et al., 2006, MNRAS, 371, 1497